Nanoscale

View Online
Dynamic Article Links

Cite this: DOI: 10.1039/c0nr00789g

www.rsc.org/nanoscale

PAPER

# Conductive indium-tin oxide nanowire and nanotube arrays made by electrochemically assisted deposition in template membranes: switching between wire and tube growth modes by surface chemical modification of the template

**Nina I. Kovtyukhova* and Thomas E. Mallouk***

***Received 22nd October 2010, Accepted 22nd November 2010***
**DOI: 10.1039/c0nr00789g**

Tin-doped indium hydroxide (InSnOH) nanowires (NWs) and nanotubes (NTs) were grown from acidic aqueous solutions of inorganic precursors in a simple one-step electrochemically assisted deposition (EAD) process inside Au-plugged anodic aluminium oxide and polycarbonate membranes. When the membranes were used without any pre-treatment, InSnOH crystals nucleated on the both the Au-cathode and pore wall surfaces. By adjusting the surface chemistry of Au or the pore walls, it was possible to switch between NW and NT growth modes. InSnOH was converted into indium tin oxide (ITO) by annealing the InSnOH-filled membranes at 300 °C. The resulting wires and tubes were characterized by field emission scanning electron microscopy, transmission electron microscopy, X-ray and electron diffraction, Auger electron spectroscopy and electrical conductivity measurements. InSnOH and ITO NWs and NTs consisted of ~25–50 nm in size crystalline grains with the cubic crystal structures of $In(OH)_3$ and $In_2O_3$, respectively, and showed essentially the same morphological features as planar ITO films made by the same method. Separate tin oxide/hydroxide phases were not observed by any of the characterization methods. After heating in air at 600 °C, the ITO NWs had resistivity on the order of 10°Ω cm. EAD is an inexpensive and scalable solution-based technique, and allows one to grow dense arrays of vertically aligned, crystalline and conductive ITO NWs and NTs.

## 1. Introduction

Nanowire (NW) and nanotube (NT) arrays are being increasingly investigated as components of energy conversion devices such as solar cells, lithium batteries, thermoelectrics, piezoelectrics, and fuel cells. Future generations of these devices may require NW and NT arrays that contain different functional materials—semiconductors, dielectrics, ferroelectrics, metals, and catalysts—organized into specific three-dimensional architectures.[1,2] The high-aspect ratio NW/NT geometry can provide a direct path for charge transport[3] and, in photovoltaic systems, more efficient collection of the photogenerated charge carriers, as well as advanced antireflective and absorption properties relative to the planar film cells.[4] Additionally, transparent semiconductor oxide NWs and NTs, such as tin-doped indium oxide (ITO), $TiO_2$ and ZnO, have potential applications as high-performance top contacts to LEDs,[5] high surface area transparent electrodes in dye-sensitized[2,6–11] and polymer[12] solar cells, fillers in transparent and conductive polymer nanocomposites[13,14] and photocatalysts.[15]

*Department of Chemistry, The Pennsylvania State University, University Park, Pennsylvania, 16802, USA. E-mail: nina@chem.psu.edu; tem5@psu.edu*

Although the unique combination of optical and electrical properties of ITO films has been known for more than 3 decades and has led to a variety of important applications, the fabrication of ITO NWs and NTs has only recently been explored.[5,7,8,11–14,16–21] The synthetic effort has mainly been focused on vapor phase methods that include vapor–liquid–solid growth,[16] carbothermal evaporation,[17] oblique electron beam evaporation,[12] pulse laser ablation,[7] molecular beam epitaxy,[5] and templated atomic layer deposition of ITO NTs.[11] The majority of vapor-phase methods produce randomly oriented arrays of good crystal quality NWs, and so far only the epitaxial growth on lattice-matched [100] yttrium stabilized zirconia substrates has resulted in well aligned vertical arrays of highly conductive single crystal NWs.[18] The practical use of these techniques, however, is limited by high energy consumption, expensive equipment, and, in the latter case, by sophisticated and expensive substrates.

Low-cost solution-based routes to ITO NWs, NTs and their arrays are now beginning to be developed. Currently these methods are represented in the literature by the solvothermal synthesis of free standing ITO NWs[19] and electrophoretic[8,20] or sol–gel[20,21] filling of porous templates. The former method gives good quality crystalline NWs of different lengths but requires further development for NW size control and alignment. The

latter template-based methods produce arrays of interconnected polycrystalline NWs[8,20] and NT sheets[21] with small (≤10 nm) crystallite size. These methods involve multistep syntheses[8,19–21] and use metal–organic precursors, which can reduce the conductivity of the resulting NWs by contamination with organic components.[20] Except for highly conducting epitaxially grown NWs ($\rho = 10^{-3}$–$10^{-5}$ Ω cm[5,18]), the reported resistivity values for ITO NWs made by other methods are in the range of 0.4–5 Ω cm,[16,20,21] which is at the higher end of the resistivity scale of ITO films prepared by various deposition techniques ($10^{2}$–$10^{-5}$ Ω cm).[22]

This paper introduces electrochemically assisted deposition (EAD) in template membranes with cylindrical pores as an alternative approach to conductive ITO NWs and NTs. Unlike conventional electrochemical deposition, EAD does not involve electron transfer between soluble precursors and the growing electrode film. Instead, it exploits electrochemical reactions for altering chemical conditions, such as the pH, in the interfacial solution/electrode zone, which causes precipitation in the vicinity of the electrode surface. Because of this, the EAD method is applicable to the deposition of insulating and poorly conducting materials. For conducting materials, EAD has some advantages over electroplating and electroless deposition; those important to this study are its applicability to materials that are not easily oxidized or reduced, and control over the thickness and morphology of the deposits by adjusting electrochemical parameters. So far, EAD has been used to grow several single-component metal oxide, hydroxide, and chalcogenide films,[23] and has been recently extended to templated synthesis of ZnO[24] and CdS[25] NWs, and ZnO[26] and $SnO_2$ NTs.[27]

Recently we reported the growth of transparent and conductive ITO films by EAD and demonstrated the applicability of the method to more complex binary metal oxides. ITO films were deposited in a one-step procedure that allowed good control over the composition and the composition-dependent electrical properties. The films had crystalline grains with the morphology and cubic crystal structure of $In_2O_3$, and there were no evidence of the presence of a separate tin oxide phase.[28] Here we extend this method to ITO NWs and NTs. We show that EAD growth in membrane pores can give arrays of either NWs or NTs. Because metal oxide/hydroxide crystals nucleate in the proximity of the electrode (but not necessarily on the electrode surface), they can adsorb on a different surface if it is located close enough to the electrode. If that surface is the pore wall, then NTs can result.[27] We observe growth on both the electrode and the pore walls, leading to porous polycrystalline ITO NWs. We show that the surface of the electrode and the pore walls can be modified by adsorbing different molecules and ions to separate the two growth modes. To the best of our knowledge, this is the first example of switching between NW and NT growth modes in an EAD process. The modification of the AAO pore walls was proven to be a successful strategy for preparing nanotubes by the direct electrochemical deposition and sol–gel techniques.[29]

## 2. Experimental section

### 2.1. Membrane preparation

Commercial anodic aluminium oxide (AAO) membranes (Anodisc 25, 0.2 μm Whatman) with real pore size of 300 ± 50 nm, and commercial polycarbonate (PC) membranes with real pore sizes of 200–250 nm (Nucleopore, Whatman, 0.2 μm) and 70 ± 10 nm (Osmonics, Inc., Poretics 0.03 μm) were used as templates. The latter two membranes are referred to below as PC(200) and PC(70), respectively. Except for experiments in which the pore walls were deliberately modified (as described below), the membranes were used as purchased. The membranes were first coated with thermally evaporated 150–200 nm thick Ag (AAO) or Au (PC) films on their open pore side. In the case of AAO membranes, 10–20 coulombs of Ag were then electroplated on top of the evaporated Ag film to make a robust base for subsequent deposition. Then short (200–300 nm) Au plugs were electroplated inside the membrane pores to serve as the cathode in the EAD synthesis.

*AAO membranes with hydrophobic pore walls and negatively charged Au-plug surfaces* were prepared as follows. A membrane with the electroplated Ag back contact was dried in vacuum at ~50 °C for 3 h and immediately placed in a octadecyltrichlorosilane (OTS), (Gelest) solution in anhydrous heptane-$CCl_4$ (14 ml heptane + 6 ml $CCl_4$ + 0.2 ml OTS) for 24 h. The membrane was then soaked in anhydrous heptane : $CCl_4$ (14 : 6 ml) for 30 min and in anhydrous cyclohexane for 20 min, and dried in an Ar stream. This very hydrophobic membrane was wetted with ethanol and 200–300 nm long Au plugs were electroplated inside the pores. The membrane was washed with $H_2O$ and the Au surface was cleaned by holding it at +0.9V for ~3 min and washing with $H_2O$. Then the Au-plug surface was made negatively charged by deposition of a monolayer of 2-mercaptoetanesulfonic acid (MESA, Aldrich) (the membrane was soaked in aq. 1 wt% MESA solution for 30 min followed by washing with $H_2O$ for ~30 min). This membrane is referred to below as AAO-OTS.

*AAO membranes with hydrophobic Au-plug surfaces and negatively charged pore walls* were prepared as follows. A membrane with the Au-plugs electroplated inside the pores was soaked in a 2.5 v% solution of 1-hexadecane thiol (HDT), (Aldrich) in anhydrous EtOH (0.25 ml HDT + 10 ml EtOH) for 24 h followed by washing with 3 portions of EtOH (~30 min) and drying in Ar. Then the membrane was soaked for 20 min in an aqueous 0.5 wt% solution of $(NH_4)_{10}W_{12}O_{41}$, washed with water and dried in an Ar stream. After this treatment, the membrane weight increased by 0.21 mg, corresponding to an estimated coverage of ~0.15 molecular monolayer (the $W_{12}O_{41}^{10-}$ ionic mass is $\sim 4.8 \times 10^{-21}$ g, its area is ~1 nm$^2$, and the surface area of the AAO membrane pore walls is ~3000 cm$^2$). This is a reasonable coverage value for $W_{12}O_{41}^{10-}$ anions that are adsorbed on the positively charged alumina pore surface. Their high ionic charge should prevent them from close packing within the monolayer. This membrane is referred to below as AAO-WOx.

### 2.2. Growth of nanowires and nanotubes

ITO NWs and NTs were grown by the method developed for the planar ITO films.[28] $In(NO_3)_3 \cdot xH_2O$ (99%, Alfa-Aesar) was dissolved in an aqueous solution of 4.6 mM $HNO_3$ (pH 2.3) with 0.1 M supporting electrolyte salt ($KNO_3$ or NaCl). Deionized water was used in all experiments. Solid $SnCl_4 \cdot xH_2O$ (98%, Alfa-Aesar) was then added to this solution. All solutions remained transparent and stable for a period of weeks (0.1 M $KNO_3$) or

days (0.1 M NaCl). However, in all EAD procedures, freshly prepared (~30 min old) solutions were used.

In a typical experiment, a Au-plugged membrane (diameter 2 cm) was used as the cathode. For an AAO membrane, the surface area of the Au plugs was estimated as ~1.4 $cm^2$ from the average pore diameter (300 nm) and pore density ($2 \times 10^9$ $cm^{-2}$, estimated by FESEM). The membrane was placed at the bottom of a cylindrical electrochemical cell equipped with a Pt counter electrode and an Ag/AgCl reference electrode. The cell was preheated to 79–80 °C in a water bath. A solution of $In(NO_3)_3$ (10 mM) and $SnCl_4$ (1–3 mM) was also preheated to 79–80 °C and placed into the cell. EAD was conducted in the potentiostatic mode at −0.5 V at 79–80 °C. The membrane was then washed thoroughly with deionized water and dried in an Ar stream. Metal hydroxide wires/tubes prepared in this way are referred to hereafter as InSnOH NWs/NTs. EAD experiments were typically performed in air. Therefore, unless otherwise stated, some amount of dissolved oxygen was always present during the reaction. When oxygen-free conditions were needed, the solution was purged with Ar for 20 min prior to deposition.

To convert InSnOH to ITO, the InSnOH-filled membranes were heated in air at 300 °C for 30–60 min.[28] For electrical measurements, the membranes were further heated at 600 °C for 30 min. Finally the AAO membranes were etched (partially or completely) with 0.1 M NaOH and PC membranes were dissolved with $CH_2Cl_2$. For experiments in which the NWs/NTs were released from the array, the Ag backing layer was dissolved in ~1M $HNO_3$ before membrane etching.

### 2.3. Characterization

Both InSnOH and ITO NWs/NTs were characterized by field emission scanning electron microscopy (FESEM, JEOL 6700F, accelerating voltage 3 kV, gun current 20 μA), transmission electron microscopy (TEM) and selected area electron diffraction (SAED) (JEOL 1200 EXII, accelerating voltage 120 kV), and X-ray diffraction (XRD, Philips X'Pert MPD, Cu-Kα radiation).

Auger electron spectra (AES) were acquired on a PHI 670 scanning Auger spectrometer. The beam energy and current were 10 keV and 10 nA, respectively. The spectra were acquired with 1 eV steps between data points. The P/P intensities of the In MNN and Sn MNN lines were calculated by using a 5 point Savitsky-Golay smooth and derivative. The In/Sn atomic ratio was estimated by using 10 keV RSF values from the PHI Handbook.[30] All calculations were performed with CASA software (Version 2.3.12Dev9).

Current–voltage characteristics were measured across the ITO NW array inside the AAO-OTS membrane in an Au/ITO/Au device configuration in air at ambient temperature (Keithley 2400 SourceMeter). The ITO NW-filled AAO-OTS membrane was partially etched from the top by 0.1 M NaOH (without sonication), washed with water and dried in an Ar stream. A small piece of Au foil (variable electrode) was placed on top of the protruding NW array, which was contacted on the bottom by the gold plugs (source electrode). The foil was pressed into the array by using a tungsten tip. The tip contact area was ~10 $\mu m^2$.

## 3. Results and discussion

Aqueous solutions of the both $In^{3+}$ and, even more so, $Sn^{4+}$ inorganic salts are known to form precipitates at neutral pH, and therefore acidic conditions of pH 2.3 were used in the EAD process. Electrochemically assisted deposition of metal oxide/hydroxide films from acidic solutions occur through the hydrolysis of soluble precursors at the appropriate pH ($pH_H$) in the vicinity of the electrode. InSnOH NWs in PC and AAO membranes were grown under the EAD conditions developed previously for planar InSnOH films on Au-substrates.[28] According to that study, bi- or polynuclear indium–tin complexes form in acidic solutions upon mixing the $In(NO_3)_3$ and $SnCl_4$ precursors. These precursor complexes favor the incorporation of tin into the crystal lattice of indium hydroxide. In this work, molar Sn/In ratios were selected from the range that gave the highest Sn content in EAD ITO films.[28] By analogy with InSnOH film growth, we consider the following reactions to contribute to InSnOH NWs growth in the membrane pores:

pH increase in the vicinity of the Au-plug in the pore:

$$NO_3^- + 2H^+ + 2e^- \rightarrow NO_2^- + H_2O \quad (1)$$

$$O_2 + 4H^+ + 4e^- \rightarrow 2H_2O \quad (2)$$

Hydrolysis of the soluble indium and indium-tin complexes in the solution as protons are removed cathodically:

$$[In(H_2O)_6]^{3+} \xrightarrow{H_2O,\ pH > 2.3} In(OH)_3(\mathbf{s}) + 3H^+ + 3H_2O \quad (3)$$

$$[(HO)_{4-n}Sn(\mu\text{-}O(OH)]_m In_n(H_2O)_{5n}]^{2n+} \xrightarrow{H_2O,\ pH>2.3} In_nSn_mO_x(OH)_v(\mathbf{s}) + H^+ \quad (4)$$

Where (**s**) indicates solid state, $n$ and $m$ may vary as $1 \leq n \leq 4m$, and $m \geq 1$. By analogy to InSnOH film growth by EAD, the kinetics of reactions 3 and 4 and the solubility of the reaction products will determine the composition of InSnOH NWs.[28] However, the kinetics may be altered by the pore geometry, relative to growth on planar electrodes.

### 3.1. Nanowire growth in the untreated AAO and PC membranes.

As shown in Fig. 1, the EAD method can be used to grow InSnOH NWs in the ~200–300 nm pores of AAO (A–C) and PC (D, E) membranes as well as in a 70 nm PC membrane (F). After careful dissolution (without sonication) of the AAO membrane, the InSnOH NWs remain attached to the Au plugs on the Ag backing film and form a densely packed NW array (Fig.1B). Although in transmission microscopy the nanowires look relatively smooth and dense (Fig.1A,D–F), FESEM images reveal a rather porous morphology (Fig. 1C; 3A,B,D).

All as-prepared InSnOH nanowires are polycrystalline and have the cubic crystal structure of $In(OH)_3$ as revealed by SAED patterns (insets in Fig.1A and D). Heat treatment of the PC and AAO membranes filled with InSnOH NWs up to 300 °C results in the thermal conversion of InSnOH to ITO NWs that are also polycrystalline and have the cubic crystal structure of $In_2O_3$

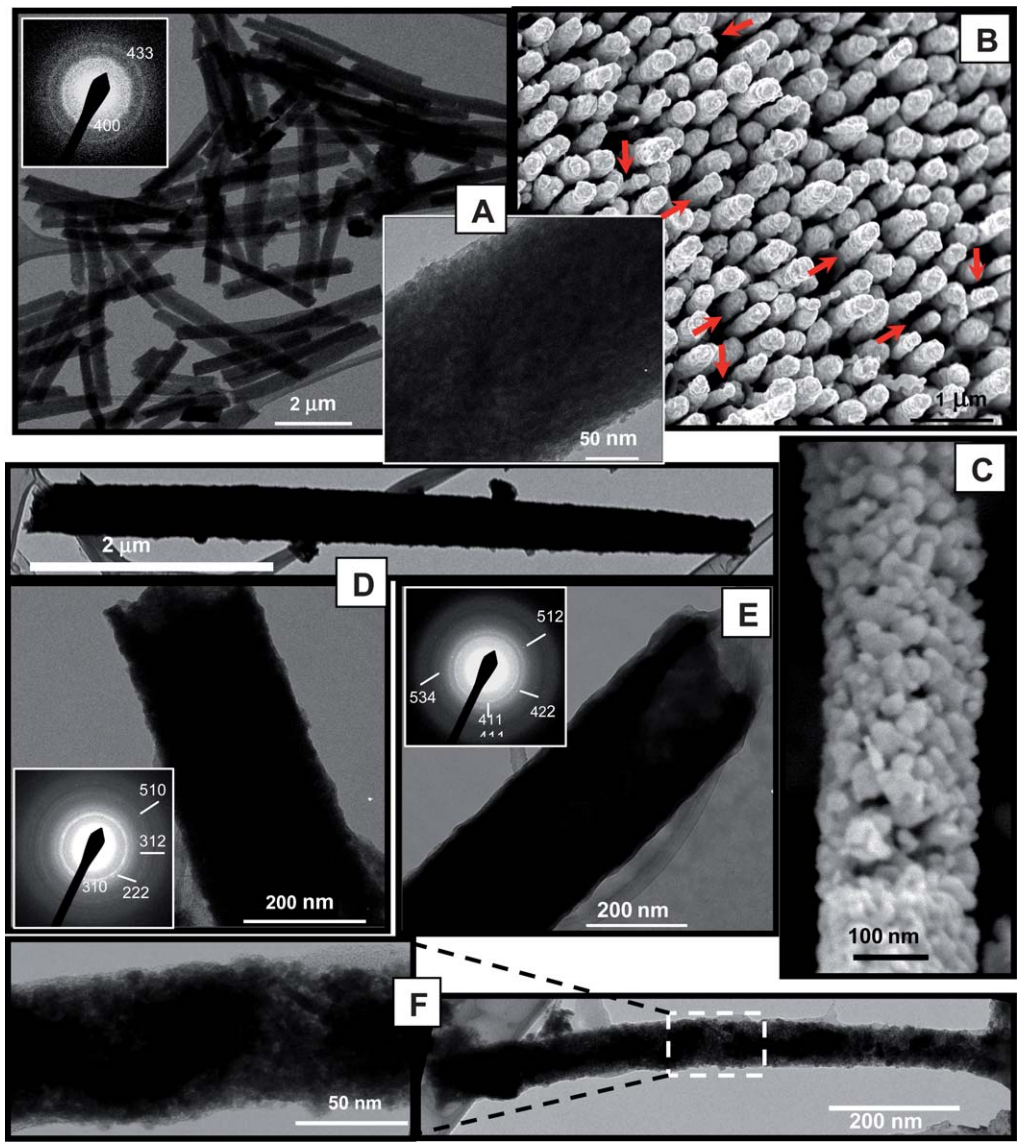


**Fig. 1** TEM (**A, D–F**) and FESEM (**B, C**) images of InSnOH NWs grown in AAO (**A**–**C**), PC(200) (**D**–**E**) and PC(70) (**F**) membranes. In **B**, red arrows indicate NWs with diameters smaller than the pore width. **C, E -** NWs heat-treated in the membrane at 700 °C and 300 °C, respectively. The insets show corresponding SAED patterns. *Deposition solutions*: (**A**, **D**, **E**) 0.1M $KNO_3$, Sn/In = 0.28–0.3; **B** –0.1M NaCl Sn/In = 0.1; (**C**, **F**) 0.1M $KNO_3$, Sn/In = 0.1.

(SAED pattern in Fig.1E). The SAED patterns show no reflections that can be assigned to tin oxide phases, consistent with XRD data from planar EAD films.[28] The absence of tin oxide reflections is characteristic of ITO films prepared by vapor- and solution-based techniques and is associated with $SnO_2$ present in the finely dispersed form.[31,32] It is important to note that AAO membranes can withstand heat treatment up to 700 °C, which gives ITO NWs with larger crystal grain size (Fig.1C *vs.* 3D).

XRD patterns of the InSnOH NWs that are still inside the membrane (*i.e.* with the NW axis oriented perpendicular to the substrate) are shown in Fig. 2. For comparison purposes a reference $In(OH)_3$ pattern[32] is shown at the bottom. Interplanar distances (*d*) and average crystal sizes (*t*) calculated from the XRD patterns are summarized in Table 1. Consistent with the SAED data, all of the InSnOH nanowire samples can be indexed to cubic $In(OH)_3$, and no reflections of tin oxide phases are seen. The NWs grown in the PC-200 membrane (Fig. 2, trace 1) reveal strong preferred orientation in the [100] direction and the cubic lattice parameter $a = 7.97$ Å (Table 1), which is in good agreement with reference data.[32] The crystallization behavior in the PC-200 membrane is very similar to that of the planar EAD InSnOH films, but the crystal grain size in the [100] direction is about half that of the films.[28] In contrast, NWs grown in AAO membranes (Fig. 2 traces 2, 3), although they have a more random distribution of crystal orientations, reveal a preferred texture in the [211] direction, which is especially well pronounced for NWs deposited from NaCl solution (trace 3). This orientation was not observed with planar EAD InSnOH films grown on Au substrates from the same solutions. The NWs also have crystals that are considerably larger in the [100] direction (Table 1). Compared to the reference data[32] and the XRD patterns of planar EAD films,[28] the AAO-grown NWs have

 

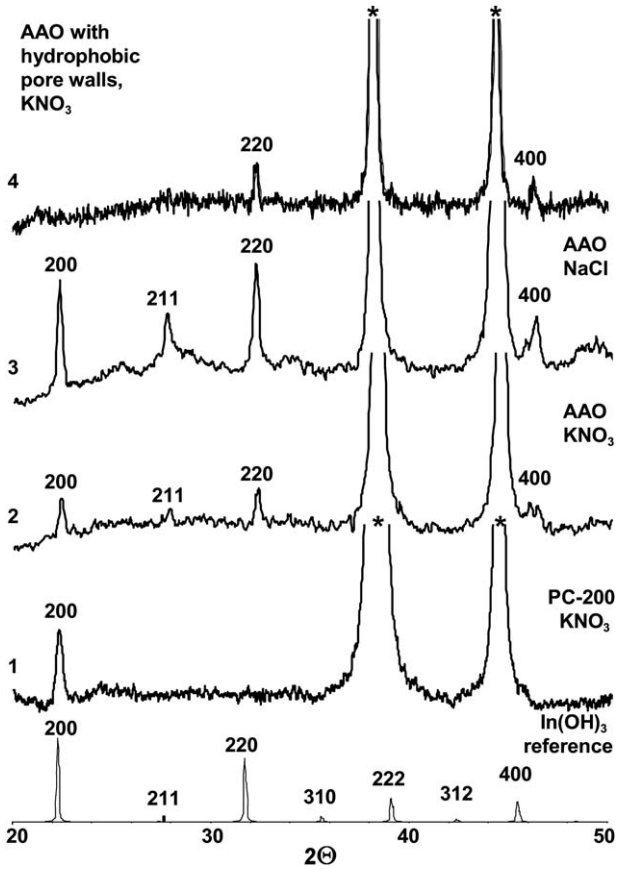


**Fig. 2** XRD patterns of PC(200) (1) and AAO (2–4) membranes filled with InSnOH nanowires. 4 – AAO membrane was pre-treated with OTS. * indicates Au reflections. Bottom: reference XRD pattern of $In(OH)_3$.[32] *Deposition solutions*: (1, 2) 0.1 M $KNO_3$, Sn/In = 0.1; (3) 0.1 M NaCl, Sn/In = 0.1; (4) 0.1 M $KNO_3$, Sn/In = 0.28.

slightly smaller unit cells (the interplanar distances are shorter by ~0.01–0.04 Å (Table 1)). It is possible that the pore geometry plays a role in the InSnOH crystallization behavior.

FESEM images of InSnOH NWs grown in the PC-200 (Fig.3A, B) and AAO (Fig.3C, D) membranes confirm different crystallization behavior inside these templates.

The main structural feature of the PC(200)-grown NWs are ~70–100 nm long bundles of ~7 nm thick rods that form densely packed NW walls and are relatively loosely packed in the central part of the wire body (Fig.3A, B). The similar bundles of rodlike crystals, although considerably larger, are also the main building blocks of the planar EAD InSnOH films (Fig. 3G). This may explain the similarity of the XRD patterns of the PC-grown NWs (Fig.1, tr.1) and the planar films. In the latter, the crystal size in the [100] direction is related to the length of the rodlike particles,[28] and it is reasonable to assign the particle size of ~25 nm in the [200] direction determined for the PC(200)-grown NWs (Table 1) to the length of the rodlike crystals in the bundles. Thus, the majority of the bundles that compose the NW body align along the wire long axis and account for the strong preferred [200] orientation (Fig.2, tr.1). Interestingly, ~8–20 nm thick single crystal ITO NWs that grow along the [100] direction have also been observed at the initial stages of the MBE deposition on Si-substrates, but no further assembly into bundles were found.[5]

Fig. 3D shows typical FESEM images of the InSnOH NWs deposited in an AAO membrane from a solution containing 0.1 M $KNO_3$. The morphology of these NWs is similar to that of the PC(200)-grown NWs in that they have dense walls and a relatively loosely packed core. The main structural features, however, are different. The NWs consist of roughly cylindrical (or prismatic) particles (rods), some of which extend from the walls toward the center (Fig. 3D, inset). The average crystal sizes of ~39 nm in the [200] direction and ~29 nm in the [220] direction (Table 1) are close to the length and width of the cylindrical features, respectively. Interestingly, we did not observe thinner rods or their bundles in any FESEM images of this type of NWs.

The structure of the InSnOH NWs grown in AAO from a solution containing 0.1 M NaCl is completely different (Fig. 3C). The wires have a dense core that is built from relatively flat polycrystalline plates with their plane oriented approximately perpendicular to the wire axis. The primary crystals that form the plates have lateral sizes close to those in the [220] and [200] direction (40–50 nm, respectively), determined from XRD patterns (Table 1). The smallest $t$ ~36 nm in the [211] direction is probably related to the thickness of the plates and may explain the preferred NW texture in this direction (Fig.2, tr.3). We should note that planar EAD InSnOH films deposited from 0.1 M NaCl solutions do not reveal any platelike particles and have the same bundle-of-rods morphology as films deposited from 0.1 M $KNO_3$ solutions.[28] This suggests that $Na^+$ and $Cl^-$ ions do not directly affect the crystal shapes.

It should be noted for all three systems (Fig. 1C and 3A–D) that there are no obvious inclusions of the amorphous phase that is characteristic of hydrous tin oxides formed under these conditions in the absence of In.

Because the PC(200) and AAO membranes have about the same pore diameters, the restricted pore geometry cannot alone be responsible for the observed differences in the NWs structure, although it could lead to the observed decrease in crystallite size relative to planar films (compare *e.g.* Fig. 3A and 3G). We have observed that ~7 nm thick rodlike particles, which tend to assemble in bundles, and flat platelike particles of InSnOH can also form in $In(NO_3)_3$–$SnCl_4$ solutions when the pH is increased by adding NaOH or tetrabutylammonium hydroxide (TBA) (Fig.3E, F). This implies that, in the EAD process, shape of the main structural features in the InSnOH NWs and films is determined by the crystallization habit of $In(OH)_3$/InSnOH species rather than by the surface on which they are deposited. The latter, however, may play a role in preferential adsorption of crystal seeds that result in the growth of a particular feature. It is also possible that larger InSnOH crystals form in the solution phase within the pore and then adsorb on a surface. In our system, the alumina or polycarbonate pore walls are in close proximity to the Au-cathode and hence there are two surfaces (for each template), Au and alumina (or polycarbonate), on which adsorption of the seeds or their precursors can occur. In the PC(200)-$KNO_3$ and AAO-$KNO_3$ systems, FESEM images (Fig. 3A, B, D) suggest that the growth of many crystals is initiated at the wall surface. In the AAO-NaCl system, adsorption on the walls is less likely to occur, judging from the wire structure and thickness. There are many NWs (indicated with red

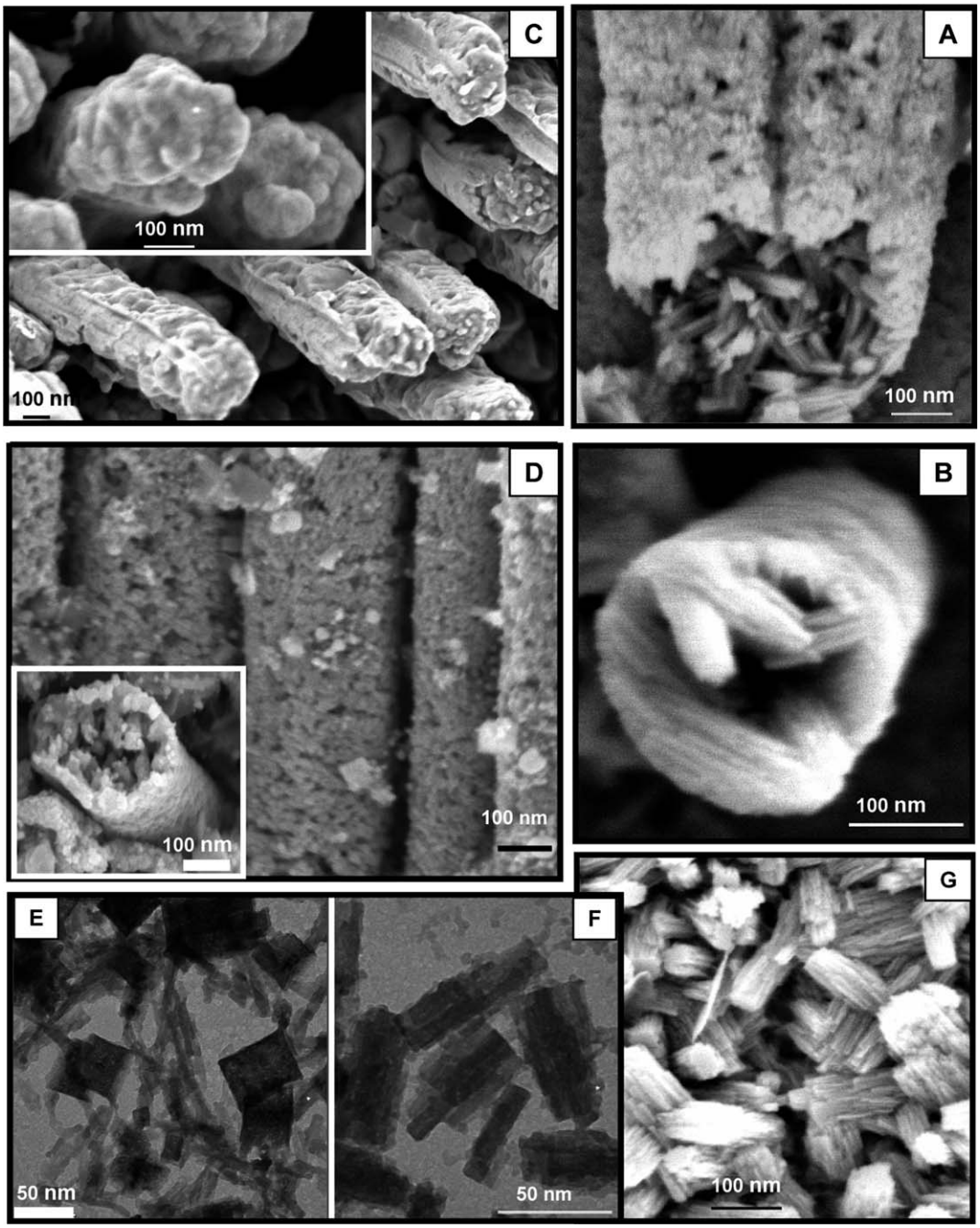


**Fig. 3** FESEM (**A–D**) of the InSnOH NWs grown in PC(200) (**A**, **B**) and AAO (**C**, **D**) membranes. The insets in **C** and **D** show top view of the same NW arrays. **E, F -** TEM of InSnOH particles grown in solution by increasing the pH with NaOH (**E**) and tetra(n-butylammonium) hydroxide (**F**) at 80 °C. **G** - typical FESEM image of an EAD InSnOH film on a Au substrate, showing bundles of rodike crystals as the main building block [for details see ref. 28. *Starting solutions*: (**A**, **B**, **D**, **G**) 0.1 M $KNO_3$, pH 2.3, Sn/In = 0.1; **C** – 0.1M NaCl pH 2.3, Sn/In = 0.1; (**E**, **F**) pH 2.3, Sn/In = 0.1.

arrows in Fig.1B) that are considerably thinner than the pore width.

It is also important to consider that the $NO_3^-$ and $H^+$ ions and $O_2$ molecules compete with InSnOH for adsorption on the Au-cathode surface and that some fraction of this surface should always be available for the pH regulating reactions (1, 2) to occur. If NW growth is initiated on both the walls and the Au surface, one would expect the porous NWs structure to allow transport of ions to the cathode. Such structures are shown in Fig. 3A, B, D). When the wire growth starts preferentially at the Au-cathode surface, then channels for ion transport may form between the wire body and the pore wall which results in thinner and denser NWs (Fig. 1B and 3C).

If this picture is correct, it suggests a means of affecting the NW structure and related properties by guiding selective adsorption processes. A remaining question is, how far from the cathode surface can InSnOH species form and adsorb on the pore walls? In an attempt to answer this question we consider the

 

**Table 1** XRD parameters of InSnOH NWs in the membrane

| | PC(200)-$KNO_3$ | | AAO-$KNO_3$ | | AAO-NaCl | | AAO-OTS | | $In(OH)_3$ Ref. 32 |
|---|---|---|---|---|---|---|---|---|---|
| [hkl] | $t^a$, nm | $d$, Å | $t^a$, nm | $d$, Å | $t^a$, nm | $d$, Å | $t^a$, nm | $d$, Å | $d$, Å |
| 200 | 24.6 | 3.985 | 38.5 | 3.97 | 48.5 | 3.985 | — | — | 3.987 |
| 211 | — | — | w | 3.21 | 35.9 | 3.21 | — | — | 3.225 |
| 220 | — | — | 28.5 | 2.78 | 39.4 | 2.78 | 39.4 | 2.77 | 2.819 |
| 400 | | w | | 1.96 | | 1.96 | | 1.96 | 1.993 |

[a] $t$ was determined from the width-at-half-maximum of the corresponding XRD reflections using the Scherrer equation.[33] The XRD pattern of $LaB_6$ powder was used as a standard.

change in the $H^+$ concentration within the pore volume for a simple system that does not contain In–Sn species or dissolved oxygen.

### 3.2. Estimation of the pH gradient along the membrane pores generated by $NO_3^-$ reduction (reaction 1)

The current transient measured with an Au-plugged AAO membrane in a solution containing 0.1M $KNO_3$ and 4.8 mM $HNO_3$ (pH~2.31) was used to estimate the pH increase within the pores (Fig. 4A graph 2). One can see that a steady state current is established within ~30s after applying the potential of −0.5 V *vs.* Ag/AgCl. The thickness of the AAO membrane is 60 μm, which is well within the thickness of the Nernst diffusion layer, NDL ($\delta$ ~100 μm in unstirred solutions), and one can use the Nernst-Plank equation to describe the ionic flux within the pore (see scheme in Fig. 4B). For one-dimensional mass-transport to an electrode, the flux of ions is expressed as a sum of diffusion, migration, and convection processes. We assume that convection is negligible inside the pores, and thus the ion flux (along the $x$-axis) can be written as

$$J_i(x) = -J_{Di}(x) - J_{Mi}(x) \quad (5)$$

Where $J_{Di}$ and $J_{Mi}$ are the diffusion and migration flux components of ion i, respectively.

For the case of the finite diffusion [$C(x > \delta, t) = C^s$] and $C(x, t = 0) = C^s$, the diffusion flux is[34]

$$-J_{Di}(0,t) = D_i[\partial C_i(x,t)/\partial x] \approx D_i(C_i^s - C_i^e)\delta \quad (6)$$

where $D$ is the diffusion coefficient, $C^s$ is the ion concentration in the bulk solution, and $C^e = C(x = 0, t)$ is the ion concentration at the outer Helmholtz plane (OHP) of the electrode surface.

The migration flux can be expressed as[34]

$$J_{Mi} = j_M/nF = \pm T_i j z_i F \quad (7)$$

where $j_M$ is the migration component of the current density, $j$, $z$ is the ionic charge, $F$ is Faraday's constant, and $T_i$ is the transport number (the fraction of the total current carried by ion i)

$$T_i = z_i u_i C_i / \sum_{j=1}^{n} z_j u_j C_j \quad (8)$$

where $u$ is the ion mobility. For a solution containing 0.1M of $KNO_3$ and 0.0048M of $HNO_3$ at 80 °C, $T_{NO_3} = 0.459$ and $T_{H^+} = 0.086$.

Taking $j = JnF$ and combining eqn (5)–(7), one can determine the concentration difference along the pore length as

$$C_i^s - C_i^e = j(1 - nT_i/z_i)\delta/nFD_i \quad (9)$$

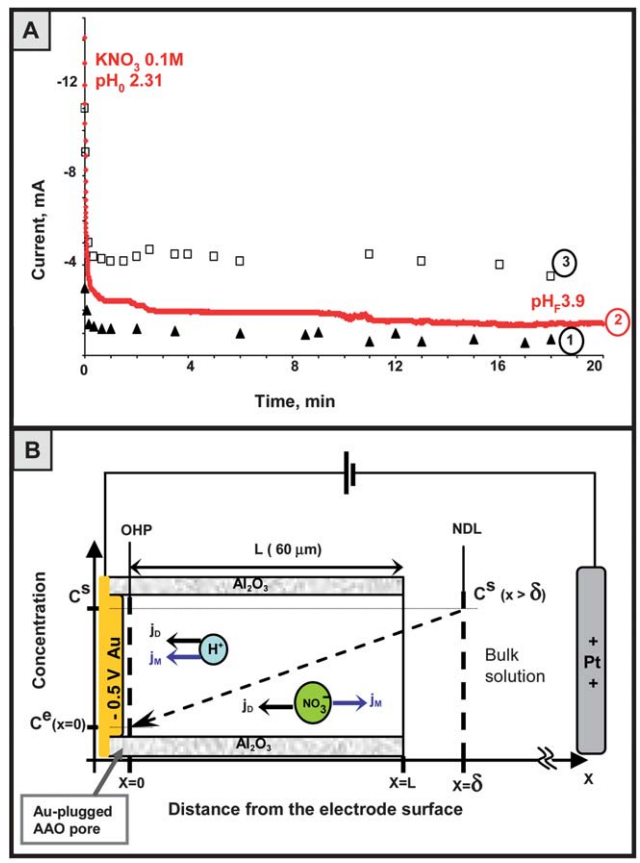


**Fig. 4** **A** - Cathodic current transients of Au-plugged AAO membrane electrodes measured in $KNO_3$ solutions (initial pH 2.31) at −0.5 V *vs.* Ag/AgCl and 80 °C. Solution compositions: (1) 0.1 M $KNO_3$, 4.8 mM $HNO_3$, 10 mM $In(NO_3)_3$, 2.8 mM $SnCl_4$; (2) 0.1 M $KNO_3$, 4.8 mM $HNO_3$, the solution was purged with Ar for 20 min prior to deposition; (3) 0.1 M $KNO_3$, 4.8 mM $HNO_3$, 2 mM $In(NO_3)_3$, 0.56 mM $SnCl_4$. 2 – $pH_o$ and $pH_f$ indicate the starting and final pH, respectively, of the bulk solution. 1, 3 – AAO membranes were pre-treated with OTS and $W_{12}O_{41}^{10-}$, respectively. **B** - Schematics of ion diffusion and concentration gradient formation along the AAO pore during the cathodic process shown in **A (tr. 2)**. OHP - outer Helmholtz plane, NDL - Nernst diffusion layer; $C^s$ and $C^e$ - ionic concentrations in the bulk solution and on the electrode (OHP), respectively; $j_D$ and $j_M$ – diffusion and migration components of the current density.

For reaction (1), the cathodic current density is determined by the flux of $NO_3^-$ anions and the charge transferred per mole of the anions.

$$j = J_{NO_3^-} nF \text{ with } n = 2 \quad (10)$$

Cathodic reaction (1) occurs in multiple steps in which one proton is transferred per electron. Thus, we can write

$$J_{H^+} = j/nF \text{ with } n = 1.$$

Note that the same conclusion applies if reaction (2) contributes to the current. Eqn (9) can then be written as

$$C_{H^+}{}^s - C_{H^+}{}^e = j(1 - 0.086)\delta/FD_{H^+} \quad (11)$$

For the current values shown in Fig.4A tr.2 and $\delta = 60\mu m$ (the pore length is used for simplicity instead of the unknown NDL thickness), the proton concentration difference $C_{H^+}{}^s - C_{H^+}{}^e$ can be estimated as $\sim 4\times10^{-4}$ M. In the range of the bulk solution pH of 2.3–3, in which hydrolysis begins (judging from stability of the precursor solutions), this creates a pH gradient of ~0.05–0.2 units along the length of the pore, or about $(0.8–3)\times10^{-3}$ pH unit per micron of pore length. This small pH gradient may be damped further by the buffering effect of the $NO_2^-$ produced in reaction (1), and by the generation of protons in reactions (3) and (4).

This calculation suggests that, because of fast proton diffusion, a very small pH gradient exists within the membrane pores. This implies that hydrolysis of the In–Sn complexes should occur almost simultaneously along the pore length once the appropriate pH ($pH_H$) is established by the cathodic electrode reaction(s).

### 3.3. Mechanism of InSnOH nanowire growth and selection of nanowire or nanotube growth mode.

Based on these calculations we suggest a mechanism for NW growth that includes four basic steps (Fig. 5A):

1. Under cathodic conditions, the concentration of the nitrate anions and protons decreases due to reactions (1) and (2), and a pH gradient forms along the pore length. The concentrations of $In^{3+}$ and $[In–O–Sn]^{2+}$ ions do not change.

2. At a certain pH, $pH_H$, hydrolysis of the soluble indium and indium–tin precursors occurs (reactions 3, 4) leading to the formation of small molecular clusters in the solution phase within the pore. At this stage the adsorption of the clusters can take place on both the Au-cathode and pore wall surfaces. The pH within the pore continue to increase, and a concentration gradient of $In^{3+}$ and $[In–O–Sn]^{2+}$ ions forms between the pore and the bulk solution.

3. The concentration of the hydroxide species in the pores increases to the point where crystals nucleate. These nuclei may adsorb on both the Au-cathode and pore wall surfaces.

4. As further hydrolysis occurs, InSnOH crystals grow from the adsorbed seeds, resulting in a porous wire. Some of the InSnOH crystals can form in the solution phase and precipitate near the bottom of the pore. This should give NWs that are denser at the bottom. We did observe this growth mode in some TEM images.

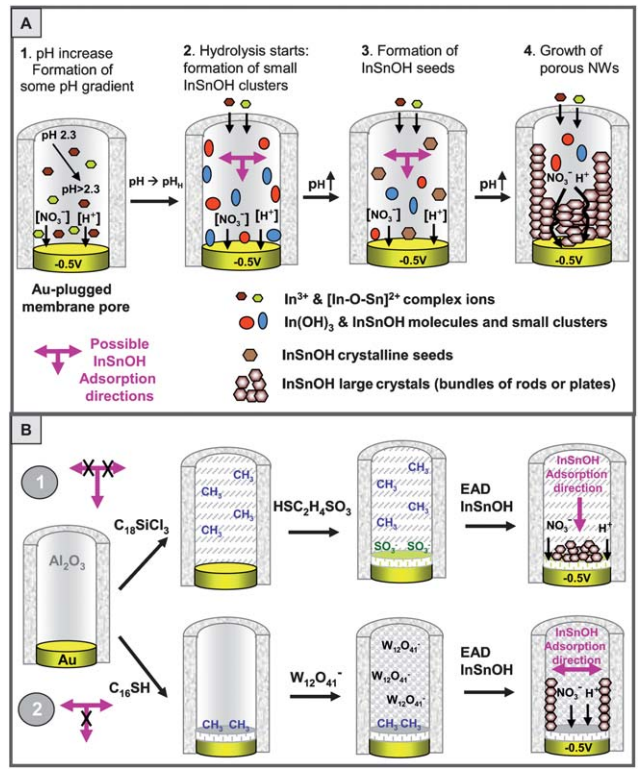


**Fig. 5** **A -** Proposed mechanism for InSnOH NW growth in membrane pore. **B -** Scheme for tuning the AAO membrane pore chemistry to switch between NW and NT growth modes.

This mechanism should allow one to manipulate the NW structure and related properties by tuning the adsorptive properties of the cathode and pore wall surfaces. To do this we exploited the different surface chemistries of the Au- cathode and the alumina pore walls (see scheme in Fig. 5B).

Two different types of AAO membranes were prepared, one with hydrophobic walls and a hydrophilic Au-cathode surface, and the other with hydrophilic walls and a hydrophobic cathode. The hydrophobic surfaces were made by selective adsorption of long-chain alkane derivatives with chlorosilyl (wall) and thiol (Au) anchoring groups. The second, negatively charged hydrophilic surface was then made by adsorbing mercaptoethanesulfonic or paratungstate anions, which adsorb selectively on the Au and alumina surfaces. Negatively charged surface modifying groups were chosen to enhance the adsorption of positively charged InSnOH species. The EAD procedure was then applied, resulting in the growth of InSnOH NWs in the AAO membrane with hydrophobic walls, AAO-OTS (Fig. 6 A–D) and InSnOH NTs in the AAO membrane with the hydrophobic Au-cathode and hydrophilic pore walls, AAO-WOx (Fig. 6G). Cathodic transients for the EAD processes in AAO-OTS and AAO-WOx membranes are shown in Fig. 4A, traces 1 and 3, respectively. One can see that the steady-state current is about 4 times higher when the NTs are formed (tr.3 *vs.* tr.1), which suggests better accessibility of the cathode surface during the NT growth, as expected from the scheme illustrated in Fig. 5B (route 2 *vs.* 1).

A typical TEM image of an InSnOH nanotube (Fig. 6G) shows that the uniformly dense NT walls are in contact with the Au-plug edge and very little crystalline material accumulates in

the center of the Au-plug surface. This supports the idea that NT growth occurs on the pore walls and not on the Au-cathode. The tube walls are largely transparent and there are no obvious crystal grains in the images. This morphology suggests that the tube walls are built from sheetlike crystals that grow parallel to the walls. This crystal morphology was observed in some planar EAD InSnOH films (Fig. 6H)[28] and InSnOH colloidal sols (Fig. 3E). Like those planar films,[28] the tube walls are polycrystalline with the cubic crystal structure of $In(OH)_3$ (SAED pattern in Fig. 6G inset).

An optical microscope image of AAO-OTS-grown NWs released from the membrane (Fig. 6 A) shows up to 20 μm long nanowire pieces. FESEM images of the top face of InSnOH-filled AAO-OTS membranes (not shown) reveal that many of the pores are completely filled. We also observed in some TEM images (not shown) NWs with shapes replicating the branched part of the AAO membrane (which is the top part of the membrane in our experiments). These observations (along with the small amount of charge passed during the EAD process (Fig. 4A, tr.1)) support the idea of almost simultaneous InSnOH formation along the pore length. Wire formation might thus include crystal growth both from the cathode and in the solution within the pores with further precipitation and/or agglomeration of the solution-born crystals. SAED (Fig. 6B inset) and XRD (Fig .2 tr.4) patterns indicate the formation of InSnOH NWs with the cubic crystal structure of $In(OH)_3$.

TEM images in Fig. 6B, C distinguish two typical morphologies with the AAO-OTS-grown NWs. One (Fig. 6B) is similar to

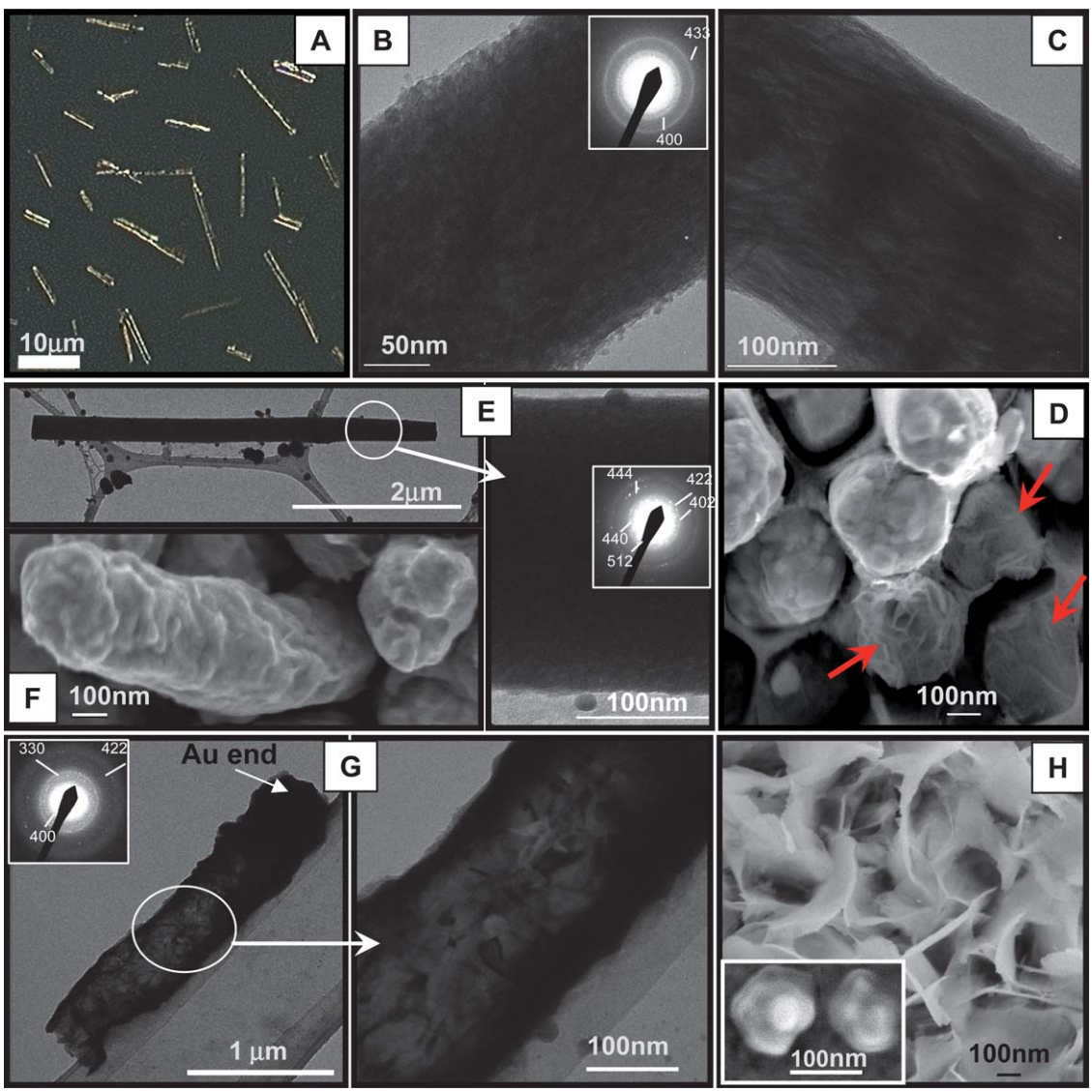


**Fig. 6** Optical microscope (**A**), TEM (**B, C, E**) and FESEM (**D, F**) images of InSnOH NWs grown in an AAO-OTS membrane. In **D**, red arrows show NWs with morphology dominated by folded sheetlike features **E, F**- NWs heat-treated in the membrane at 600 °C. **G** -Typical low and higher resolution TEM images of InSnOH NTs grown in an AAO-WOx membrane. **H** - FESEM image of an EAD InSnOH film on a Au substrate, showing a morphology dominated by sheetlike features; the inset shows a typical crystal pattern that was observed in the initial stages of growing planar InSnOH films. The insets in **B**, **E**, **G** show corresponding SAED patterns. *Deposition solutions*: (**A**–**G**) 0.1 M $KNO_3$, pH 2.3, Sn/In 0.28; (H)–pH 2.3, Sn/In 0.1; inset - 0.1 M $KNO_3$, pH 2.3, Sn/In 0.1.

that observed for NWs grown in untreated AAO membranes (Fig. 1A) and the other (Fig. 6C) reveals some fibrous features inside the core of the wires. FESEM images of InSnOH NWs in partially dissolved AAO-OTS membranes (Fig. 6D) also show two distinct morphologies. One (indicated with red arrows in Fig. 6D bottom-center, right) reveals folded sheets that resemble the sheetlike particles observed with planar EAD InSnOH films (Fig. 6H).[28] Comparing Fig. 6C and 6D, it appears that the fibrous features in the TEM images are likely to be edges of thin sheets that appear in the FESEM images.

The second morphology observed with AAO-OTS-grown NWs has relatively thick horizontal platelike features (top-center, left). This morphology is very similar to that of NWs deposited from NaCl solutions (Fig. 3C). Although platelike crystals were not found on the surface of the planar EAD InSnOH films (for any solution compositions),[28] we did observe them in the initial stages of film deposition (Fig. 6H, inset). In the case of planar EAD films, these crystals were likely overgrown by bundles of rods at later stages, but in the case of NWs, these features persist along the wire length. Here, the pore-restricted geometry is likely to play a role. The plates seem to be characteristic of NWs whose crystallization is initiated at the Au-cathode surface and not at the pore walls. While seed adsorption on the pore walls was weakened purposefully in the AAO-OTS membranes, weak adsorption of $Cl^-$ ions on the untreated AAO walls may occur with NaCl electrolytes. Interestingly, despite their morphological similarity and similar crystal size (Table 1), NWs from the AAO-OTS membrane have a preferred [220] texture (Fig. 2 tr.4) *versus* the [211] preferred orientation of the NWs grown from NaCl solutions (Fig. 2 tr.3). FESEM images (Fig. 6D) also show that the NWs do not adhere to the AAO-OTS membrane pore walls and that there is some space between the pore walls and the NW surface.

Heating of the AAO-OTS grown NWs at 600 °C leads to the ITO NWs with the cubic crystal structure of $In_2O_3$ (Fig.6E, inset), and morphology of the ITO similar to that of the InSnOH NWs (Fig. 6E, F).

Auger electron spectra of the ITO NWs deposited into the AAO-OTS and PC(200) membranes from $KNO_3$ solutions with Sn/In molar ratios of 0.28 and 0.3, respectively, are shown in Fig. 7. The atomic Sn/In ratios in the NWs are estimated as 0.034 and 0.039 for AAO-OTS and PC(200) respectively. It should be noted that planar EAD films deposited from the same solutions had the Sn/In ratios of ~0.08–0.09,[28] which is ~2.3 times higher. The lower Sn/In ratios in the NWs are unlikely to be caused by the chemical treatment of the AAO membrane or the post-deposition membrane etching because the AAO-OTS (etched with 0.1M NaOH) and the untreated PC(200) (etched with $CH_2Cl_2$) grown NWs have very similar ratios. By analogy with planar EAD films,[28] the kinetics of reactions 3 and 4 and the solubility of the reaction products should determine the compositions of InSnOH NWs. It appears that the restricted pore geometry can change some of the relevant rates (including possibly the diffusion rates). Further study of these effects is needed to control the Sn/In ratios in EAD NWs and NTs.

### 3.4. Electrical properties of ITO NWs

Current–voltage (*iV*) characteristics were measured with AAO-OTS-grown ITO NWs, which had the densest polycrystalline

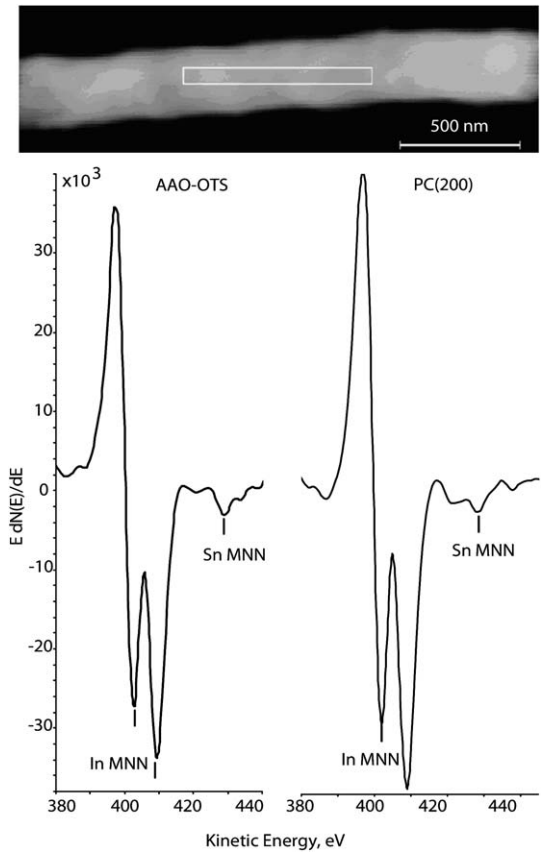


**Fig. 7** 10 keV Auger electron spectra of ITO NWs grown in an AAO membrane treated with OTS (left) and an untreated PC(200) membrane (right). Top: SEM image of an ITO NW with a white box indicating the scan area. The Sn/In atomic ratios represent the average of three measurements on different NWs for each membrane type. *Deposition solutions*: 0.1 M $KNO_3$, pH 2.3, Sn/In 0.28 (AAO-OTS) and 0.3 (PC-200).

structure. The device configuration is shown schematically in Fig. 8, top. After partial dissolution of the membrane a small piece of gold foil was pressed into the NW array surface by means of a tungsten tip with a contact area of ~10 $\mu m^2$. A typical top view of such a NW array (Fig. 8A) reveals that the NWs have somewhat different heights. This fact and the rough surface of the W-tip implies that only a few NWs will form a good electrical contact within the 10 $\mu m^2$ area of the top electrode and contribute to the observed current.

A typical *iV* characteristic of an ITO NW array sandwiched between two gold electrodes shows rectifying behavior (Fig. 8B), which was reproducible for all six measurements performed on this device. For the *iV* curve shown here, the reverse/forward resistance ratio is $R_R/R_F = 10$ at 1.5 V and the rectification ratio at 50 V is ~170. The turn-on potential in the forward bias mode (top Au-electrode negative) is ~0.7 V, which suggests the formation of a Schottky barrier at the Au/ITO interface (the difference in work functions of Au and ITO is ~0.7–1 V). The bottom Au/ITO-NW contact is much more resistive, which may be a result of either the formation of a resistive layer at the Au/ITO interface or an increase in the Au cathode work function during the EAD process. Qualitatively similar rectifying behavior was observed with about 80% of the planar EAD ITO film devices.[28] This rectifying behavior, although not completely

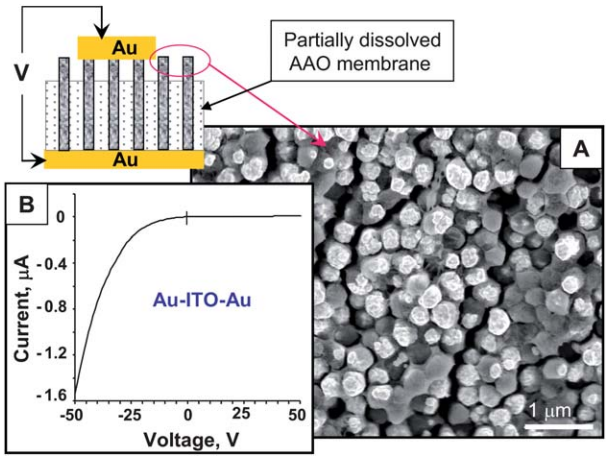


**Fig. 8** *iV* characterization of ITO nanowires grown in AAO-OTS membranes and heated at 600 °C. Top - schematic of the device configuration. **A** - top view (FESEM) of the ITO NW array after partially dissolving the AAO membrane. Top Au-foil contact (variable) was pressed into this surface by a tungsten tip. **B** - typical *iV* curve measured on the ITO NW array. Resistance of the ITO NWs was calculated for linear regions of the *iV* curves as the average of six different locations on top of the array.

understood, could find useful applications in its own right. It can also be eliminated by removing the bottom contact. Past the turn-on potential, the resistance drops by several orders of magnitude. The average electrical resistance calculated from the linear region of six *iV* curves taken at different locations was ~25 MΩ. Taking the device thickness as ~60μm and the NW diameter as ~200 nm (pore diameter in the top branched part of the AAO membrane) we estimated the resistivity of the ITO NWs as 1.3 Ω cm, assuming that a single NW makes a contact with the top Au-foil electrode; the resistivity is proportionally higher if more NWs are involved. This value is in rough agreement with the resistivity of EAD ITO films, 48.5 Ω cm, with a similar Sn/In ratio of 0.029.[28] Another source of error in this measurement is the unknown channel width for a single NW, (*i.e.* the cross sectional area, which varies along the wire length). Judging from FESEM images (*e.g.* Fig. 6F), the roughly parallel horizontal crystal plates that constitute the NW body are shifted relative to each other, which brings the channel width below 200 nm. In light of these uncertainties, we can estimate that the resistivity of the ITO NWs is in the range of 0.4–5 Ω cm reported for ITO NWs in the literature,[16,20,21] and is consistent with the range of data reported for ITO films with similar Sn/In molar ratios.[22] We note that there is a room for improvement in the conductance of EAD ITO NWs by optimizing the Sn/In ratio and the post-synthesis heat treatment. The highest conductivity of the EAD ITO films was found with an Sn/In ratio of ~0.09–0.1.[28] Further study of the kinetics of reactions 3 and 4 in the membrane pores will be needed to gain better control over the NW composition.

## 4. Conclusions

Nanocrystalline InSnOH and ITO NWs and NTs were grown in AAO and PC template membranes, extending the EAD method to high aspect ratio binary metal oxides. EAD offers advantages over other methods for growing ITO, because it is an inexpensive and simple one-step procedure that produces dense arrays of vertically aligned, crystalline NWs and NTs.

FESEM, XRD, and SAED data show that InSnOH NWs and NTs have morphological features similar to those of planar InSnOH films and the same cubic crystal structure of $In(OH)_3$. Thermal treatment of the as-deposited InSnOH wires and tubes in air at 300 °C leads to the formation of corresponding ITO structures with the cubic crystal structure of $In_2O_3$, which is typical for ITO films. As in the EAD ITO films, there is no evidence of the presence of a separate tin oxide/hydroxide phases and it is assumed that Sn is dispersed at the atomic level in the $In_2O_3$ crystals. AES analysis indicates a Sn/In atomic ratio of ~0.034–0.039 for wires deposited in AAO and PC membranes, respectively, which is ~2.3 times lower than the Sn/In ratio of planar films deposited from the same solutions. This implies different kinetics for hydrolysis or mass transport in the membrane pores. The resistivity of the ITO NWs has been estimated at ≥1.3 Ω cm for a Sn/In atomic ratio of ~0.034. Although the resistivity of the nanowires is in the range of values reported for ITO NWs prepared by other methods, and for some ITO films with similar Sn/In molar ratios, it may be possible to increase the conductivity by optimizing the Sn/In ratio and the post-synthesis heat treatment.

Porous polycrystalline NWs with dense walls form from nitrate solutions when AAO and PC membranes are used without chemical treatment of their pore walls. The rapid diffusion of protons in the pores results in only a small gradient in pH, and thus the nucleation of InSnOH can occur on either the cathode or pore wall surfaces. Based on this finding, we adjusted surface chemistry of the walls and the cathode in order to favor adsorption and crystal nucleation on only one of the two surfaces. This approach allows one to tune the EAD process to grow either ITO NWs or NTs.

## Acknowledgements

FESEM and AES analyses were conducted at the Materials Characterization Laboratory of the Pennsylvania State University. We thank Vince Bojan for acquiring the AES spectra and for helpful discussions. This work was supported by the Office of Basic Energy Sciences, Division of Chemical Sciences, Geosciences, and Energy Biosciences, Department of Energy under contract DE-FG02-07ER15911.

## References

1 (*a*) Z. L. Wang and J. H. Song, *Science*, 2006, **312**, 242; (*b*) D. N. Futaba, K. Hata, T. Yamada, T. Hiraoka, Y. Hayamizu, Y. Kakudate, O. Tanaike, H. Hatori, M. Yumura and S. Iijima, *Nat. Mater.*, 2006, **5**, 987; (*c*) C. K. Chan, H. Peng, G. Liu, K. McIlwrath, X. F. Zhang, R. A. Huggins and Y. Cui, *Nat. Nanotechnol.*, 2007, **3**, 31; (*d*) G. K. Mor, K. Shankar, M. Paulose, O. K. Varghese and C. A. Grimes, *Nano Lett.*, 2006, **6**, 215; (*e*) M. S. Dresselhaus, G. Chen, M. Y. Tang, R. G. Yang, H. Lee, D. Z. Wang, Z. F. Ren, J. P. Fleurial and P. Gogna, *Adv. Mater.*, 2007, **19**, 1043.
2 M. Law, L. E. Greene, J. C. Johnson, R. Saykally and P. D. Yang, *Nat. Mater.*, 2005, **4**, 455.
3 S. Chung, J.-Y. Yu and J. R. Heath, Silicon Nanowire Devices, *Appl. Phys. Lett.*, 2000, **76**, 2068.
4 L. Tsakalakos. In: *Nanotechnology for Photovoltaics*, Tsakalakos, L. (Ed.) CRS, Boca Raton, 2010, Ch.6.

5 C. O'Dwyer, M. Szachowicz, G. Visimberga, V. Lavayen, S. Newcomb and C. Sotomayor-Torres, *Nat. Nanotechnol.*, 2009, **4**, 239.
6 O. Lupan, V. Guerin, I. Tiginyanu, V. Ursaki, L. Chow, H. Heinrich and T. Pauporte, *J. Photochem. Photobiol., A*, 2010, **211**, 65.
7 E. Joanni, R. Savu, M. Goes, P. Bueno, J. Freitas, A. Nogueira, E. Longo and J. Varela, *Scr. Mater.*, 2007, **57**, 277.
8 H.-W. Wang, C.-F. Ting, M.-K. Hung, C.-H. Chiou, Y.-l. Liu, Z. Liu, K. Ratinac and S. Ringer, *Nanotechnology*, 2009, **20**, 055601.
9 K. Zhu, N. Neale and A. Miedaner, *Nano Lett.*, 2007, **7**, 69.
10 A. Martinson, J. Elam, J. Hupp and M. Pellin, *Nano Lett.*, 2007, **7**, 2183.
11 A. Martinson, J. Elam, J. Liu, M. Pellin, T. Marks and J. Hupp, *Nano Lett.*, 2008, **8**, 2862.
12 P. Yu, C.-H. Chang, M.-S. Su, M.-H. Hsu and K.-H. Wei, *Appl. Phys. Lett.*, 2010, **96**, 153307.
13 H. Miyazaki, T. Ota and I. Yasui, *Sol. Energy Mater. Sol. Cells*, 2003, **79**, 51.
14 C. Capozzi and R. Gerhardt, *Adv. Funct. Mater.*, 2007, **17**, 2515.
15 L. Tan, M. Kumar, W. An and H. Gao, *ACS Appl. Mater. Interfaces*, 2010, **2**, 498.
16 (*a*) Q. Wan, Z. Zong, P. Feng and T. Wang, *Appl. Phys. Lett.*, 2004, **85**, 4759; (*b*) S. Li, C. Lee, P. Lin and T. Tseng, *Nanotechnology*, 2005, **16**, 451; (*c*) Y. Chen, J. Jiang, B. Wang and J. Hou, *J. Phys. D: Appl. Phys.*, 2004, **37**, 3319.
17 P. Nguen, H. Ng, J. Kong, A. Cassel, R. Quinn, J. Li, J. Han, M. Mcneil and M. Meyyappan, *Nano Lett.*, 2003, **3**, 925.
18 (*a*) Q. Wan, M. Wei, D. Zhi, J. MacManus-Driscoll and M. Blamire, *Adv. Mater.*, 2006, **18**, 234; (*b*) Q. Wan, P. Feng and T. Wang, *Appl. Phys. Lett.*, 2006, **89**, 123102; (*c*) Q. Wan, E. Dattoli, W. Fung, W. Guo, Y. Chen, X. Pan and W. Lu, *Nano Lett.*, 2006, **6**, 2909.
19 D. Yu, D. Wang, W. Yu and Y. Qian, *Mater. Lett.*, 2003, **58**, 84.
20 S. Limmer, S. Cruz and G. Cao, *Appl. Phys. A: Mater. Sci. Process.*, 2004, **79**, 421.
21 Y. Aoki, J. Huang and T. Kunitake, *J. Mater. Chem.*, 2006, **16**, 292.
22 (*a*) P. Nath and R. Bunshah, *Thin Solid Films*, 1980, **69**, 63; (*b*) P. Nath, R. Bunshah, B. Basol and O. Staffsud, *Thin Solid Films*, 1980, **72**, 463; (*c*) M. Buchanan, J. Webb and D. Williams, *Appl. Phys. Lett.*, 1980, **37**, 213; (*d*) J. Ederth, P. Heszler, A. Hultaker, G. Niklasson and C. Granqvist, *Thin Solid Films*, 2003, **445**, 199; (*e*) R. Tahar, T. Ban, Y. Ohya and Y. Takahashi, *J. Appl. Phys.*, 1998, **83**, 2139.
23 (*a*) J. Switzer, *J. Am. Ceram. Soc. Bull.*, 1987, **66**, 1521; (*b*) S. Limmer, E. Kulp and J. Switzer, *Langmuir*, 2006, **22**, 10535; (*c*) K.-C. Ho, *J. Electrochem. Soc.*, 1987, **134**, 52C; (*d*) C. Natarajan and G. Nogami, *J. Electrochem. Soc.*, 1996, **143**, 1547; (*e*) M. Izaki and T. Omi, *Appl. Phys. Lett.*, 1996, **68**, 2439; (*f*) S. Peulon and D. Lincot, *Adv. Mater.*, 1996, **8**, 166; (*g*) H. Minoura, T. Kajita, K. Yamaguchi, Y. Takahashi and D. Amalnerkar, *Chem. Lett.*, 1994, 339; (*h*) S. Peulon and D. Lincot, *J. Electrochem. Soc.*, 1998, **145**, 864; (*i*) C. Levi-Clement, A. Katty, S. Bastide, F. Zenia, I. Mora and V. Munoz-Sanjose, *Phys. E.*, 2002, **14**, 229; (*j*) R. Tena-Zaera, J. Elias, G. Wang and C. Levi-Clement, *J. Phys. Chem. C*, 2007, **111**, 16706.
24 M. Lai and D. Riley, *Chem. Mater.*, 2006, **18**, 2233.
25 (*a*) D. Xu, Y. Xu, D. Chen, G. Guo, L. Gui and Y. Tang, *Adv. Mater.*, 2000, **12**, 520; (*b*) N. I. Kovtyukhova, B. K. Kelley and T. E. Mallouk, *J. Am. Chem. Soc.*, 2004, **126**, 12738–12739.
26 L. Li, S. Pan, X. Dou, Y. Zhu, X. Huang, Y. Yang, G. Li and L. Zhang, *J. Phys. Chem. C*, 2007, **111**, 7288.
27 (*a*) M. Lai, J. Martinez, M. Gratzel and J. Riley, *J. Mater. Chem.*, 2006, **16**, 2843; (*b*) M. Lai, J. Lim, S. Mubeen, Y. Rheem, A. Mulchandani, M. Deshusses and N. Myung, *Nanotechnology*, 2009, **20**, 185602.
28 N. I. Kovtyukhova and T. E. Mallouk, *Chem. Mater.*, 2010, **22**, 4939.
29 (*a*) J. C. Hulteen and C. R. Martin, *J. Mater. Chem.*, 1997, **7**, 1075–1087; (*b*) G. R. Patzke, F. Krumeich and R. Nesper, *Angew. Chem., Int. Ed.*, 2002, **41**, 2446–61.
30 K. Childs, B. Carlson, L. LaVanier, J. Moulder, D. Paul, V. Stickle and D. Watson, (Ed.) C. Hedberg, *Handbook of Auger Electron Spectroscopy*, Physical Electronics Inc, Eden Prairie, MN, 1995.
31 (*a*) H. Lehman and R. Widmer, *Thin Solid Films*, 1975, **27**, 359; (*b*) S.-S. Kim, S.-Y. Choi, C.-G. Park and H.-W. Jin, *Thin Solid Films*, 1999, **347**, 155; (*c*) G. Frank, H. Kostlin and A. Rabenau, *Phys. Status Solidi A*, 1979, **52**, 231.
32 ICSD: *The inorganic crystal structure database*; FIZ Karlsruhe & NIST: PC Version Release 2009/2.
33 B. D. Cullity. *Elements of X-Ray Diffraction*; Addison-Wesley: Reading, MA, 1978; pp 284–285.
34 G. Inzelt. In: Scholz, F. (Ed.) *Electroanalytical Methods*; Springer: Berlin, 2002; pp.29–48.


 